Optical Fiber Technology 55 (2020) 102139

Contents lists available at ScienceDirect

Optical Fiber Technology

journal homepage: www.elsevier.com/locate/yofte

A high sensitivity dual-parameter sensor based on glycerin filled fine-core polarization maintaining photonic crystal fiber

Ji Wang, Li Pei*, Jianshuai Wang, Zuliang Ruan, Tigang Ning, Jingjing Zheng, Jing Li

Key Lab of All Optical Network & Advanced Telecommunication Network of EMC, Institute of Lightwave Technology, Beijing Jiaotong University, Beijing 100044, China

ARTICLE INFO

Keywords:
Fine-core polarization maintaining photonic crystal fiber
Sensor
Dual-parameter
Glycerin

ABSTRACT

A high sensitivity dual-parameter sensor based on glycerin filled fine-core polarization maintaining photonic crystal fiber is proposed and verified experimentally. The sensor is fabricated by melting a fine-core photonic crystal fiber (PCF), which has a diameter of 80 μm and two single-mode fibers to form the interferometric structure. By observing the shift of the interference spectrum fringes, external strain and temperature changes can be obtained. Before the glycerin liquid is filled into the air hole, results suggest that sensitivity of the sensor in strain is 2.28 pm/με and sensor is temperature insensitive. At the same time, wavelength shift and dual-parameter change have a good linear relationship. Besides, sensitivity of proposed sensor can be improved by filling glycerin into PCF. When duty cycle N is equal 100%, linear response is also obtained and sensitivities increase to 2.98 pm/με and 237.57 pm/°C, respectively. The experiment also proved that the liquid filling duty ratio N will affect the sensitivity of the sensor. Proposed two-parameter matrix can effectively overcome the problem of sensor cross-sensitivity. The sensor has advantages of small volume, compact structure and high sensitivity.

1. Introduction

Research on sensing technologies is of great importance in many fields such as mechanical engineering, chemical industries and structural health monitoring. Compared with traditional sensors based on electrical techniques, which cannot meet the requirements of sensing applications in complicated environments, optical fiber sensor has advantages of anti-electromagnetic interference, corrosion resistance, power consumption and high sensitivity [1,2]. It has broad application prospects and has been a hot research topic in recent years. Fiber-optic sensors based on different operating principles have also been demonstrated, such as Mach-Zehnder interferometer [3–5], fiber grating [6–8], multi-core fiber [9], etc. With the maturity of photonic crystal fiber fabrication technology, photonic crystal fiber is more and more widely used in the field of sensing. Compared with single-mode fiber, PCF has the characteristics of controllable dispersion, good nonlinear effect and excellent birefringence. Because of these novel and excellent characteristics, PCF has a great application prospect in the fields of high power optical transmission, fiber laser, nonlinear optics, fiber communication and fiber devices [10–12]. As the sensor, PCF has very weak temperature sensitivity, which can reduce or even avoid the influence of temperature cross. At the same time, the sensitivity can be improved by using the air hole structure. Various new photonic crystal fibers have been proposed using the special structure and light guiding mechanism of photonic crystal fibers [13,14]. Some type of micro-structured fiber sensors with different structures can be developed and applied to the measurement of temperature [15–17], strain [18] and other parameters [19–21]. In addition, there are many air holes in the structure of the photonic crystal fiber. It is possible that liquid can be injected into the air hole. Nature characteristics of the liquid changes with external parameters varying, thereby changing the transmission of light in the core [22,23]. Filling liquids of different properties is a very effective way to improve the sensitivity of fiber sensor. Compared with the previous photonic crystal fiber sensor, this study uses a fine-core polarization maintaining photonic crystal fiber with a diameter of 80 μm to maintain polarization and increasing sensitivity. Experimental results suggest that the sensor has a high sensitivity in strain and sensor is temperature insensitive.

In this study, an interferometric sensor based on glycerin filled fine-core polarization maintaining photonic crystal fiber is proposed. Strain and temperature experiments are performed on photonic crystal fiber. According to the wavelength drift displayed by the optical spectrum analyzer, the strain sensitivity of the sensor is 2.28 pm/με, the linearity is 0.999. Compared with other sensors of the same type [24], the structure proposed in this paper has higher sensitivity. The temperature sensitivity is 3.06 pm/°C, which can be seen as insensitive to outside

* Corresponding author.
E-mail address: lipei@bjtu.edu.cn (L. Pei).

https://doi.org/10.1016/j.yofte.2020.102139
Received 1 July 2019; Received in revised form 30 December 2019; Accepted 3 January 2020
1068-5200/ © 2020 Elsevier Inc. All rights reserved.

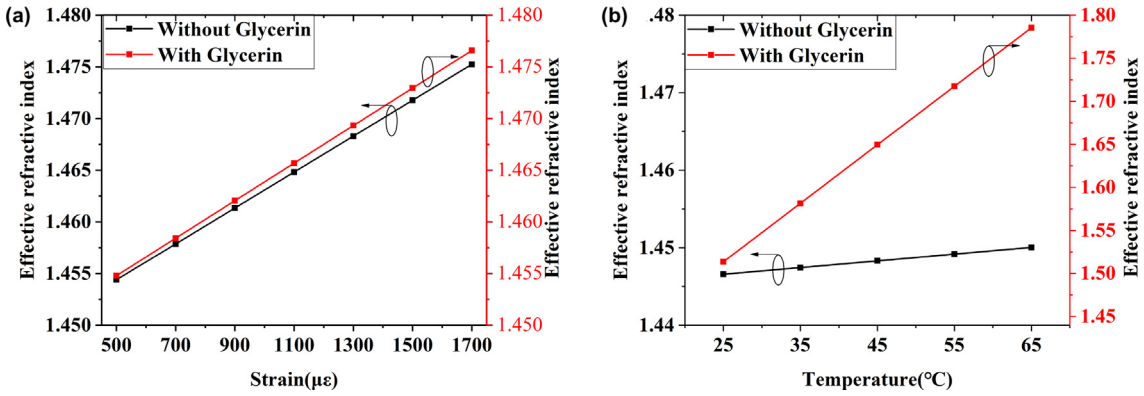

Fig. 1. Relationship between refractive index and strain (a); temperature (b).

temperature and consistent with previously reported [24]. After filling the glycerin liquid into the photonic crystal fiber, the sensitivity of strain and temperature are increased significantly, which are 2.98 pm/με and 237.57 pm/°C. Filling glycerol can make the sensor sensitive to external temperatures while maintaining high strain sensitivity, broadening the range of applications for the sensor. The proposed two-parameter matrix can effectively overcome the problem of sensor cross-sensitivity. This is a method to solving the problem that the sensor is affected by the temperature factor in the strain measurement.

2. Principle

The fiber mode interferometer is an all-fiber interference device with excellent performance, and is widely used in the fields of optical fiber sensing and optical fiber communication. This type of interferometer requires special structure to achieve splitting and combining of modes. Incident light emitted by the Amplified Spontaneous Emission (ASE) broadband source passes through the fusion of the single-mode fiber and the photonic crystal fiber, and part of the energy of the core mode is coupled into the PCF cladding, thereby exciting the cladding mode. Due to the different transmission paths of the core mode and the cladding mode, a phase difference is generated between the core mode and the cladding mode, which forms interference fringes. After the interferometer is placed in the environment to be tested, the influence of the external environment changes on the core mode and the cladding mode is different, so that the phase difference of the two paths changes, resulting in the drift of the interference fringes. By measuring the amount of drift of the interference fringes, the measurement of changes in the external environment parameters can be achieved.

Strain is an important physical quantity for monitoring the quality of buildings and bridges, which has a strong application value in reality. Assuming that strain ε is applied to sensor, changes in effective refractive index and length of sensor are Δn_{eff} and ΔL, which lead to interference spectrum wavelength shifts $\Delta\lambda$. The elastic coefficients of the core and cladding modes are defined as $p_{\varepsilon 1}$ and $p_{\varepsilon 2}$:

$$p_e = \frac{(L/n_{eff})dn_{eff}}{dL} \tag{1}$$

The Δn_{eff} and ΔL caused by strain are:

$$\Delta n_{eff} = (p_{e1} * n_{eff}^{co} - p_{e2} * n_{eff}^{cl}) * \varepsilon \tag{2}$$

$$\Delta L = L * \varepsilon \tag{3}$$

The total phase shift is equal to the sum of effective refractive index and length respectively [25–28]:

$$\begin{aligned}\Delta\varphi &= \Delta\varphi_1 + \Delta\varphi_2 \\ &= \frac{2\pi}{\lambda} * [\Delta n_{eff} * \Delta L + (p_{e1} * n_{eff}^{co} * \varepsilon - p_{e2} * n_{eff}^{cl} * \varepsilon) * L]\end{aligned} \tag{4}$$

$$\Delta\lambda = \frac{FSR * \Delta\varphi}{2\pi} = \lambda * \left(1 - \frac{p_{e1} * n_{eff}^{co} - p_{e2} * n_{eff}^{cl}}{\Delta n_{eff}}\right) \tag{5}$$

The free spectral range (FSR) decreases with increasing of interference length and effective refractive index difference. The refractive index and diameter of fiber will vary as external temperature changes, which will cause the drift of the interference spectrum fringes. The strain applied to the sensor in this experiment is small, so the changes in fiber length can be negligible.

The influence of temperature on effective refractive index corresponds to the thermo-optic effect of fiber. It is considered that the thermo-optic coefficient of fiber material is constant, so refraction index changes with temperature can be expressed as:

$$\Delta n = \xi * n * \Delta T \tag{6}$$

where ξ is the thermal coefficient of the fiber. Therefore, change of phase and wavelength caused by the temperature can be expressed as:

$$\begin{aligned}\Delta\varphi &= 2\pi * n_{eff} * L/\lambda \\ &= \frac{2\pi}{\lambda} * [\Delta n_{eff} * \alpha * L * \Delta L + (\xi_1 * n_{eff}^{co} - \xi_2 * n_{eff}^{cl}) * \Delta T * L]\end{aligned} \tag{7}$$

$$\begin{aligned}\Delta\lambda = \frac{FSR * \Delta\varphi}{2\pi} = \frac{\lambda}{\Delta n_{eff} * L}[\Delta n_{eff} * \alpha * L + (\xi_1 * n_{eff}^{co} - \xi_2 * n_{eff}^{cl}) * L] \\ * \Delta T\end{aligned} \tag{8}$$

where α is the thermal expansion coefficient of the fiber, L is the initial length of the fiber, and ΔT is the amount of temperature change.

Fig. 1(a) shows the calculated relationship between strain and refractive index. Fig. 1(b) is a graph of temperature and refractive index. It can be seen from the figure that the strain sensitivity is basically unchanged because the glycerin solution has negligible effect on the elastic coefficient. The thermo-optic coefficient of the glycerol solution is much larger than that of SiO_2, which causes the temperature sensitivity is greatly increased. Subsequent experiments also verified this phenomenon.

When strain and temperature are simultaneously applied to the sensor, shifts in different wavelength can be expressed using a matrix as [29]:

$$\begin{pmatrix}\Delta\lambda_A \\ \Delta\lambda_B\end{pmatrix} = \begin{pmatrix}K_{S,A} & K_{T,A} \\ K_{S,B} & K_{T,B}\end{pmatrix}\begin{pmatrix}\Delta S \\ \Delta T\end{pmatrix} \tag{9}$$

where $\Delta\lambda_A$ and $\Delta\lambda_B$ represent the wavelength shifts of two dips in interference spectrum, respectively. K_S and K_T are sensitivity coefficients corresponding to strain and temperature. ΔS and ΔT are the changes of strain and temperature, respectively. The strain and temperature sensitivities can be obtained as:

$$\begin{pmatrix}\Delta S \\ \Delta T\end{pmatrix} = \frac{1}{K_{S,A} * K_{T,B} - K_{T,A} * K_{S,B}}\begin{pmatrix}K_{T,B} & -K_{T,A} \\ -K_{S,B} & K_{S,A}\end{pmatrix}\begin{pmatrix}\Delta\lambda_A \\ \Delta\lambda_B\end{pmatrix} \tag{10}$$

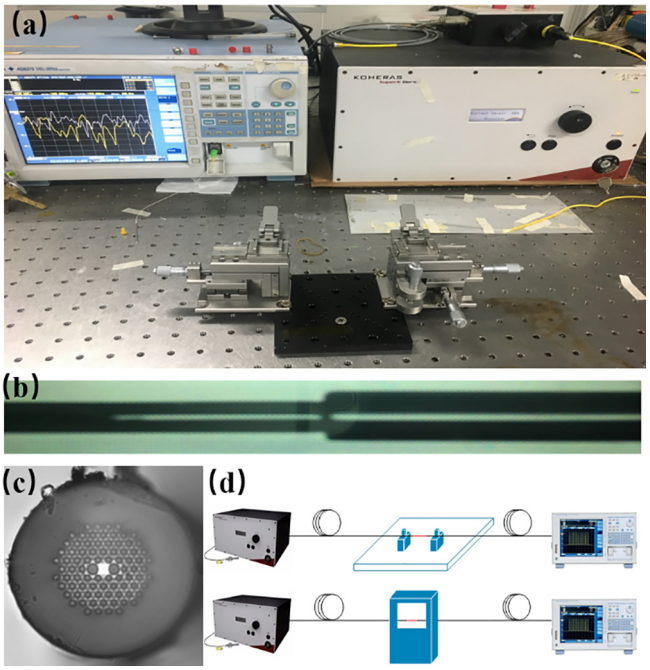

Fig. 2. Photonic crystal fiber cross section (a); propagation mode distribution (b); structure (c).

3. Experiment

The experiment diagram is shown in Fig. 2(a). Incident light emitted by the Amplified Spontaneous Emission (ASE KOHERAS, SuperK Uersa) broadband source passes through the photonic crystal fiber (PCF), and interference spectrum is observed in the optical spectrum analyzer (OSA, YOKOGAWA AQ6375). The light source outputs supercontinuum light with a wavelength range of 600 nm–1800 nm. The light emitted by the broadband light source is input into the single mode fiber and transmitted as the form of the fundamental mode. After entering PCF, the light is passed through the single-mode fiber to enter the spectrometer to observe the interference spectrum. Since the diameter of the PCF is different from the standard single-mode fiber, the fiber-optic fusion machine manual mode can only be used to adjust the aligned PCF and the single-mode fiber, and maintain the proper spacing, then finally weld. In order to obtain a stable and high extinction ratio interference spectrum, we optimized the core offset, two fibers spacing, alignment center, welding current, welding time and other parameters between single-mode fiber (SMF) and PCF, and finally obtained the sensor, as shown in Fig. 2(b). The left is a polarization maintaining photonic crystal fiber with a diameter of 80 μm, and the right is a common single-mode fiber.

The difficulty of making the sensor mainly lies in the fusion splice loss with the single-mode optical fiber and the collapse of the air hole. This structure uses a thin-core fiber, which has high stress sensitivity and does not need to be tapered or biased. In the experiments, the welding difficulty is reduced. A few key steps are listed below to ensure that the fusion point of the photonic crystal fiber has high strength and low loss, and avoid collapse.

a. End face pretreatment. The ends of the photonic crystal fiber is cleaned and cut.
b. Fix and align. The ends of the photonic crystal fiber to be fused are fixed on the clamp of the fusion machine.
c. Welding. The fusion splicer discharges the fusion ends of the photonic crystal fiber.

The cross-sectional structure is shown in Fig. 2(c). The bright part in the middle is core and the dark part around is air hole. Diameter of PCF is about 80 μm and about 4.5 cm in length. The reason for choosing thin-core fiber is that its diameter is only 80 μm, which can effectively reduce the size of the device. At the same time, a smaller diameter means that it is more sensitive to external strain changes and can increase its strain sensitivity. The central large air hole has a diameter of 3.7 μm and a hole pitch of 9 μm, while surrounding small air holes have a diameter of 1.6 μm and a period of 4.4 μm. The refractive index difference is 0.0002, which means it is a typical polarization-maintaining photonic crystal fiber. The photonic crystal fiber axial strain and temperature sensing experimental structure diagram is shown in Fig. 2(d). The strain experiment fixed the sensing part to the strain frame, and the temperature experiment placed the sensing part in the temperature control box.

As shown in Fig. 3(a), the experimental results are obtained that the spectrum of zero strain at room temperature (about 25 °C). It can be seen that the extinction ratio of the interference spectrum is not equal at different wavelengths, which is due to the existence of multiple modes in the PCF and the problem of fusion technology. A certain degree of coupling occurs between the different modes. Fig. 3(b) shows that the Fourier transform of the interference spectrum. In addition to the presence of a higher intensity peak, there are many lower intensity peaks, indicating that the interference spectrum is superimposed by many modes. Next, we select two different dip point A as the experimental point and point B as the reference point in Fig. 3(a) as the measurement wavelength, and study the sensing characteristics.

The photonic crystal fiber axial strain sensing experimental device is shown in Fig. 2(d). Input single-mode fiber is connected to the

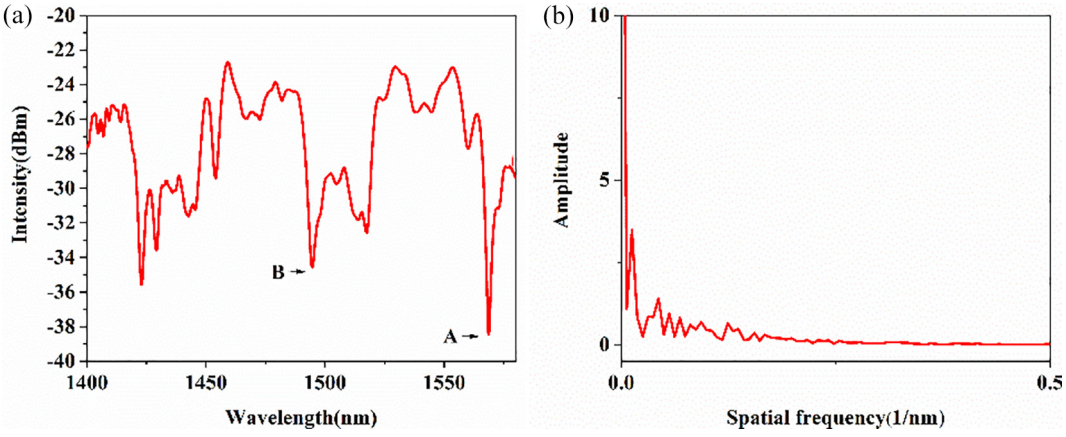

Fig. 3. Spectrum (a) and spatial spectrogram (b) of proposed sensor at room temperature without strain.

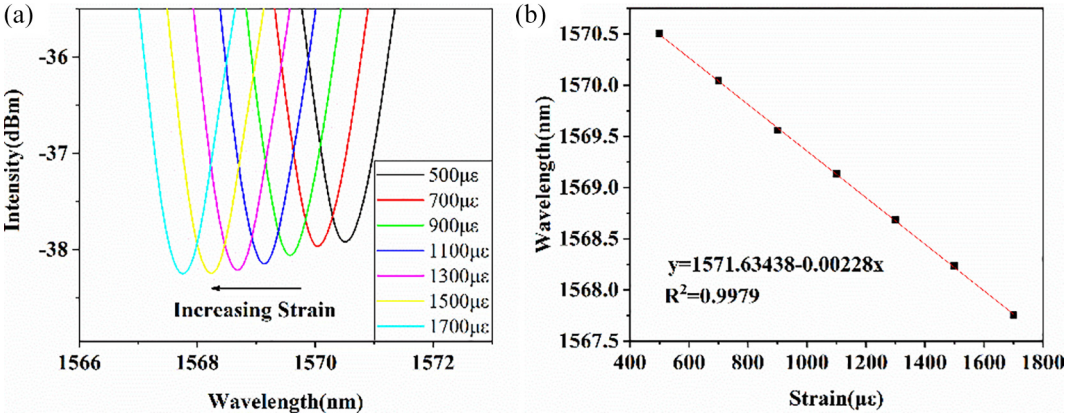

Fig. 4. Photonic crystal fiber strain sensing characteristics interference spectrum at axial strain of 500 με, 700 με, 900 με, 1100 με, 1300 με, 1500 με, 1700 με (a); linear linearity of strain when axial strain is from 500 με to 1700 με (b).

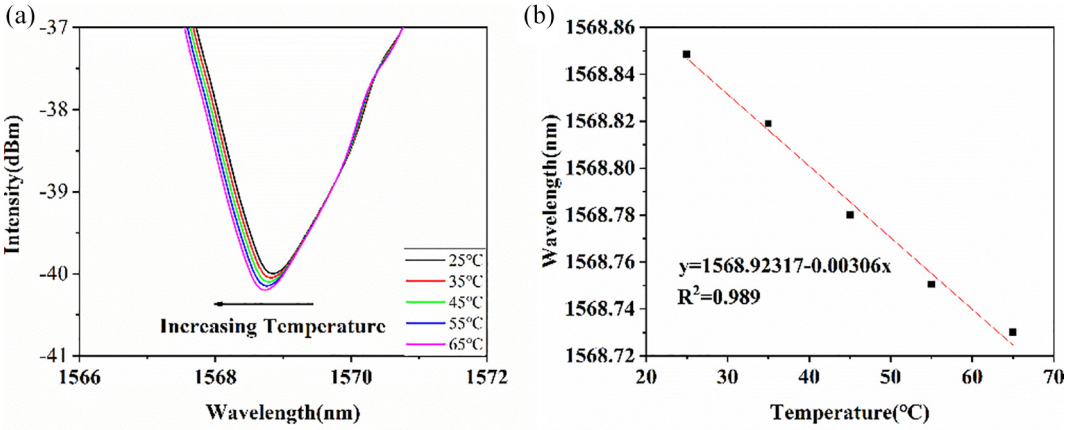

Fig. 5. Photonic crystal fiber temperature sensing characteristics interference spectrum at 25 °C, 30 °C, 35 °C, 40 °C, 45 °C (a); temperature linear fitting from 25 °C to 45 °C (b).

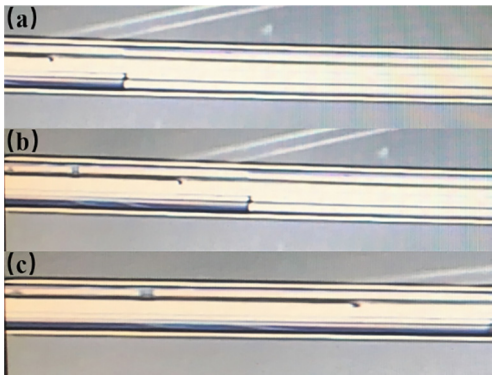

Fig. 6. Photonic crystal fiber after filling glycerin. N = 25% (a); N = 50% (b); N = 100% (c).

broadband light source, and output single-mode fiber is used to connect spectrometer. The structural parameters of photonic crystal fiber interferometer used are the same as above. Taking the photonic crystal fiber fixed in the fixture of the strain adjustment frame and naturally straightened, and recorded as 0 με state. The photonic crystal fiber is located in the middle of the two fiber clamps, and red portion is the photonic crystal fiber. The strain adjustment frame is composed of a fixed portion and a movable portion. Minimum scale of the displacement platform is 0.01 mm, and movable portion can realize three axial movements of X-Y-Z by adjusting the knob. Adjusting longitudinal and lateral knobs so that the movable portion and the fixed portion are at the same height and angle, then adjusting axial knob to simulate the axial strain change applied to fiber.

In this experiment, the distance between fixed platform and movable platform is about 11.2 cm, the displacement of each tuning is 0.01 mm, the corresponding strain change interval is 200 με, the maximum strain change is added to 2000 με, relying on the mechanical mechanism of the fiber. The strength is related too large to cause breakage of the fiber fusion joint. Room temperature condition is fixed at 25 °C. When every time the knob is adjusted, shifts is recorded after waiting for the interference spectrum to stabilize. Fig. 4(a) shows that drift of point A as a function of external axial strain. It can be concluded that as the axial strain increases, the trough shifts to the short wavelength. That is, the spectrum shifts blue, which is consistent with the previously reported photonic crystal fiber sensor. This is because the interference length increases and the effective index difference between modes decreases, when an axial strain is applied to the sensor. However, the increase speed of the interference length is far less than the decrease speed of the effective index difference caused by the elastic-optical effect, so the interference spectrum moves to the direction of short wavelength. Fig. 4(b) shows that relationship between strain and wavelength drift. When strain increases from 500 με to 1700 με, the wavelength moves a total of 2.751 nm. The seven sets of data are linearly fitted, indicating that strain change and wavelength change are approximately linear. The sensitivity of the photonic crystal fiber sensor is 2.28 pm/με and the linearity is 0.9979 by fitting. Since the photonic crystal fiber has a diameter of only 80 μm, when it is welded to a common single-mode fiber, a tapered structure is formed, which significantly increases the stress sensitivity. Compared with other sensors

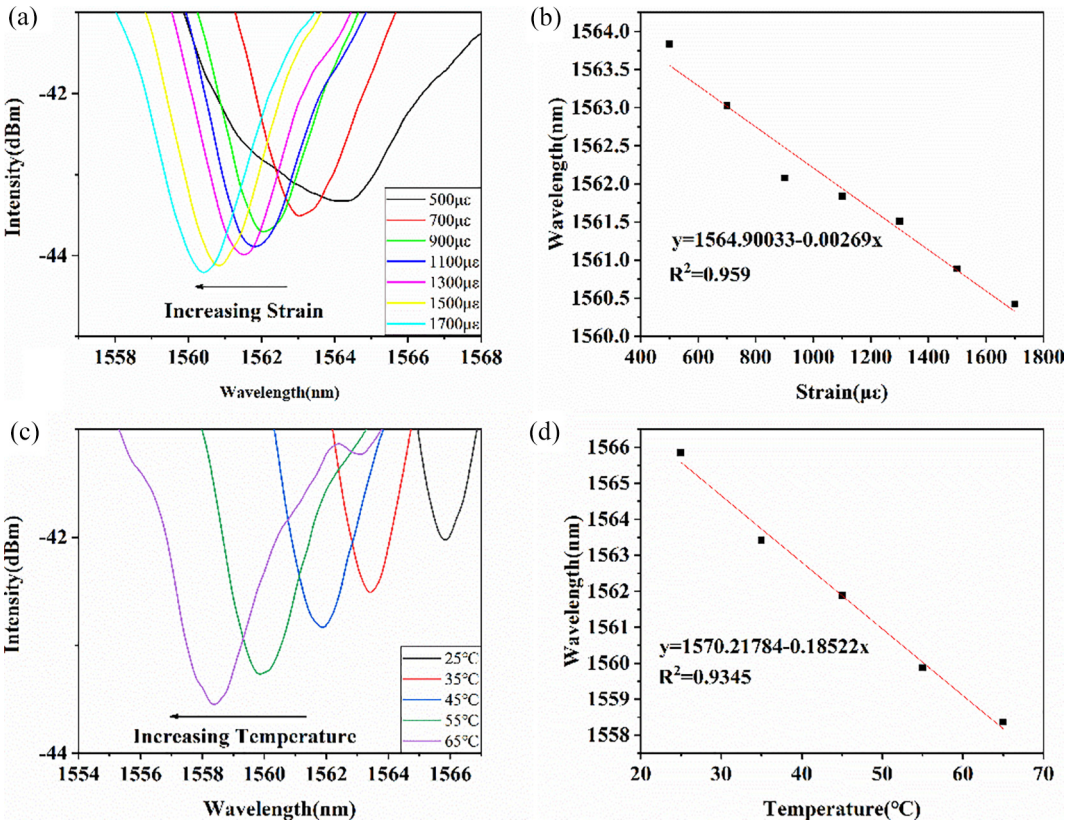

Fig. 7. When N is equal to 50%, strain sensing characteristics at axial strain of 500 με, 700 με, 900 με, 1100 με, 1300 με, 1500 με, 1700 με (a); linear linearity of strain when axial strain is from 500 με to 1700 με (b); temperature sensing characteristic interference spectrum at 25 °C, 35 °C, 45 °C, 55 °C, 65 °C (c); temperature linear fitting from 25 °C to 65 °C (d).

of the same type [24], the structure proposed in this paper has higher sensitivity. Simultaneously, there is no need for additional methods of biasing or tapping to improve the robustness of the sensor.

The photonic crystal fiber temperature sensing experimental device is shown in Fig. 2(d). Firstly, sensor part is fixed on the glass plate so that ensure the thermo-optic coefficient similar to optical fiber. The sensing part and the welded joint are twisted and stretched, then the glass plate is placed in temperature control box ((Weiss WTI) –180/40), and fixed firmly to avoid shaking the glass when temperature is raised. Minimum resolution of the temperature control box is 0.1 °C, and temperature sensing characteristics are studied by controlling temperature.

In this experiment, temperature is raised from 25 °C to 65 °C, and each time temperature is raised to 10 °C. When temperature raised to be measured, the measurement is performed after the interference spectrum is stabilized. It can be concluded from Fig. 5(a) that during the temperature rising, shifts of point A move a little to short wavelength. The interference pattern keeps almost unchanged and the measured transmission dips under different temperatures are almost overlapped when the temperature changes from 25 °C to 65 °C. The ultra-low thermal characteristic of the sensor is attributed to the low expansion coefficient α and low effective thermos-optic coefficient ξ. Experimental results show that when the temperature is over 25 °C, a slight shift for the transmission dip can be observed. The temperature influence on the interferometer can be neglected when it is operated in normal environmental condition without very large temperature variations. Fig. 5(b) shows the relationship between temperature change and wavelength drift. When temperature rises 40 °C, the wavelength has changed by 0.11856 nm, and the wavelength drift and temperature change are approximately linear. The linear sensitivity of the photonic crystal fiber sensor is 3.06 pm/°C and the linearity is 0.989.

Once all sensitivity coefficients are obtained from the experimental results. Point B is used as a reference point, and the sensitivity is tested under the same conditions. The sensitivity of point B is 2.15 pm/με and 2.97 pm/°C. Eq. (10) can be rewritten with the achieved strain and temperature sensitivities, which is given by:

$$\begin{pmatrix}\Delta S\\ \Delta T\end{pmatrix} = -\frac{1}{0.045}\begin{pmatrix}2.97 & -3.06\\ -2.15 & 2.28\end{pmatrix}\begin{pmatrix}\Delta\lambda_A\\ \Delta\lambda_B\end{pmatrix} \tag{11}$$

It shows that the discrimination between strain and temperature could be achieved for this sensor. When the proposed sensor operates within the linear range described above and the wavelength resolution of 10 pm, our proposed sensor provides the strain of 4.3 με and the temperature resolution of 3.27 °C.

Next, the glycerin solution is filled into the air hole of photonic crystal fiber. The reason why the glycerin solution is selected is that the refractive index of the glycerin solution is determined by its concentration. The suitable concentration can be adjusted to meet the conditions of photonic crystal fiber transmission. In this experiment, a 40% concentration glycerin solution is prepared and the refractive index is about 1.3841, which is lower than the refractive index of core (about 1.44). This ensures that the photonic crystal fiber light transmission conditions are not destroyed. Above all, a small amount of glycerin solution is taken out into a glass container. After the coating is entirely removed, one port of the photonic crystal fiber is placed in a glycerin container and the other is placed in air. Due to the capillary phenomenon, glycerin solution will be sucked into the air hole of the photonic crystal fiber. It is observed under the microscope after the liquid filled fiber is completely stable. As shown in Fig. 6, a clear boundary line can be seen, which means glycerin have entered the photonic crystal fiber. The air hole on the left side of the interface is filled with glycerin, and the right side of the interface is still air. The amount of liquid filled is proportional to the fill time. The Fig. 6 shows photonic crystal fibers with different duty cycles N (ratio of liquid fill

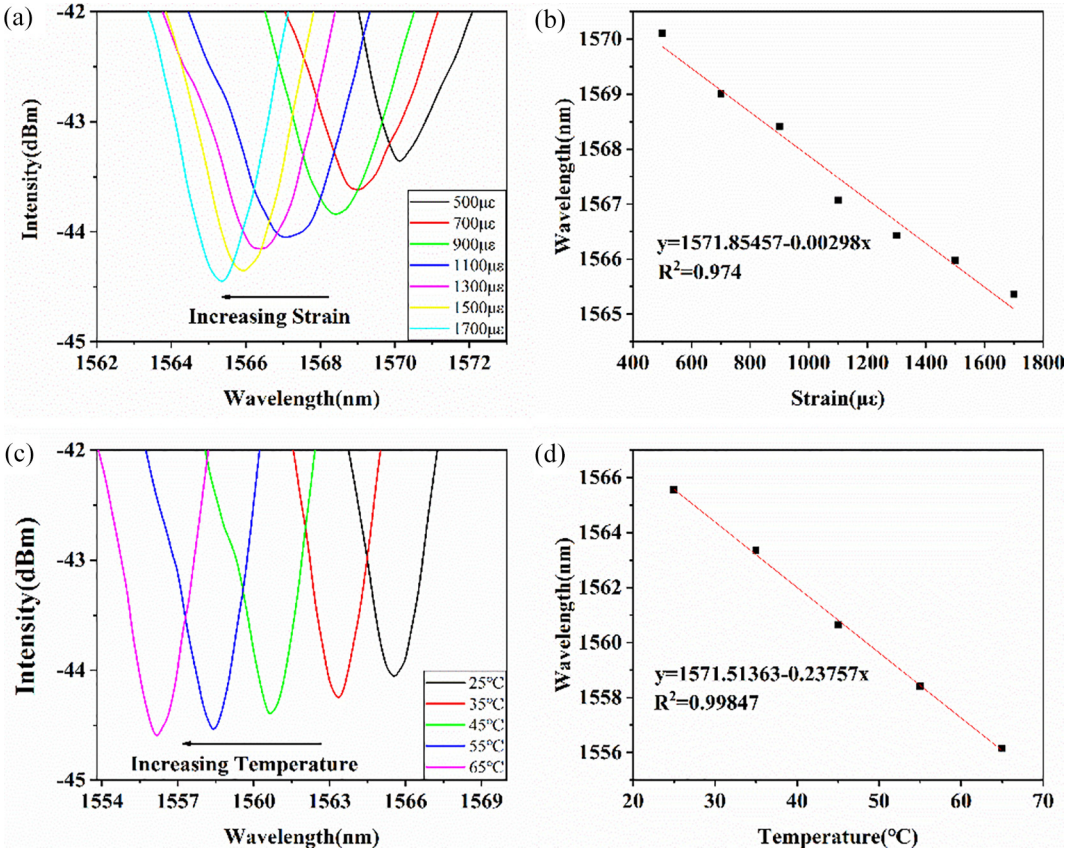

Fig. 8. When N is equal to 100%, strain sensing characteristics at axial strain of 500 με, 700 με, 900 με, 1100 με, 1300 με, 1500 με, 1700 με (a); linear linearity of strain when axial strain is from 500 με to 1700 με (b); temperature sensing characteristics interference spectrum at 25 °C, 35 °C, 45 °C, 55 °C, 65 °C (c); temperature linear fitting from 25 °C to 65 °C (d).

Table 1
Comparison of the sensitivity of different sensors.

Ref	Strain (pm/με)	Temperature (pm/°C)
[30]	1.95	–
[31]	2.14	35.2
[32]	2	34.3
[33]	1.27	49
[34]	2.21	55.2
This work	2.98	237.57

length to fiber length). Next, two ports of it are respectively fused with the single-mode fiber to form the sensor. Finally, strain and temperature sensing is performed as described above to explore the relationship between duty cycle N and sensitivity.

When N is equal to 50%, Fig. 7(a) shows that drift of the interference spectrum wavelength as a function of external axial strain. It can be seen that as the axial strain increases, the trough shifts to short wavelength. When strain increases from 500 με to 1700 με, the wavelength moves a total of 3.40 nm. The seven sets of data are linearly fitted, indicating that the strain change and the wavelength change are approximately linear. Fig. 7(b) shows that relationship between strain and wavelength drift. The linear photonic crystal fiber sensor has a sensitivity of 2.68 pm/με and a linearity of 0.959. Compared with unfilled sensor, the strain sensitivity has not improved much, but it has remained at a high level. Fig. 7(c) shows the temperature sensing experiment after filling the glycerin. When temperature rises from 25 °C to 65 °C, the wavelength of interference spectrum moves 7.484 nm to the short wavelength direction. Compared with unfilled fiber, the sensor changes from temperature insensitive to could be affected by ambient temperature. This is because the solution has a much higher thermo-optic coefficient than silica. Changes in ambient temperature affect the effective refractive index of the cladding, which is manifested by the apparent drift of the valleys on the spectrometer. Taking 25 °C as the reference point, the change of the drift with temperature is shown in the Fig. 7(d). The temperature sensitivity increased by three orders of magnitude, which reached 185 pm/°C.

When N is equal to 100%, Fig. 8(a) and (b) show that the wave trough shifts to the direction of short wavelength, with a total movement of 4.74 nm. Strain sensitivity continues to increase while maintaining good linearity. The linear photonic crystal fiber sensor has a sensitivity of 2.98 pm/με and a linearity of 0.974. It can be concluded from Fig. 8(c) that during the temperature rising, shifts of point A move to short wavelength approximately 9.40 nm. Taking 25 °C as the reference point, the change of the drift with temperature is shown in the Fig. 8(d). The temperature sensitivity increased by three orders of magnitude, which reached 237.57 pm/°C. As the amount of liquid increases, the influence of external temperature on the refractive index of the air hole of the photonic crystal fiber will also increase. When N changes from 0 to 50, the response of sensor to temperature changes insensitive to sensitive. When N changes from 50 to 100, the temperature sensitivity of the sensor can be significantly improved. It can be concluded that filling the glycerol liquid in the air hole allows the photonic crystal fiber to be used in applications where temperature is required, and the filling amount can effectively control its sensitivity.

Under the same conditions, the B point is still used as a reference point. The sensitivity of point B is 2.15 pm/με and 2.97 pm/°C. Dual-parameter sensitivities matrix also can be calculated after two sensitivity coefficients are obtained from the experimental results:

$$\begin{pmatrix}\Delta S\\ \Delta T\end{pmatrix} = \frac{1}{26.8826}\begin{pmatrix}235.43 & -237.57\\ -2.84 & 2.98\end{pmatrix}\begin{pmatrix}\Delta\lambda_A\\ \Delta\lambda_B\end{pmatrix} \quad (12)$$

It shows that discrimination between strain and temperature could be achieved when glycerin is filled into air hole. When the proposed sensor operates within the linear range described above and the wavelength resolution of 10 pm, our proposed sensor provides the strain of 3.35 με and the temperature resolution of 0.04 °C. According to the above formula, by monitoring the two valley variations of the polarization-maintaining photonic crystal fiber interference spectrum, the diversification of strain and temperature can be obtained. This is a method to solving the problem that the sensor is affected by the temperature factor in the strain measurement.

The comparison of sensitivity of different sensors is represented by Table 1. According to Table 1, it can be seen that in the optical fiber sensor that measures two parameters simultaneously, the structure proposed by this work has higher strain sensitivity. At the same time, due to the addition of a glycerin solution, the photonic crystal fiber is affected by temperature, which expands its working conditions.

4. Conclusion

In summary, an interferometric sensor based on glycerin filled polarization maintaining photonic crystal fiber is proposed and verified experimentally. External strain and temperature have changed and shift of the interference fringe can be observed. It is possible to measure these parameters by simply monitoring the wavelength shifts. The focus of this experiment is to improve sensor performance to meet the needs of higher sensitivity. Experimental results show that the sensitivities of the sensor in strain and temperature are 2.28 pm/με and 3.06 pm/°C, while the linearity is 0.997 and 0.989, respectively. Due to the use of a fine-core photonic crystal fiber having a diameter of 80 μm, it has higher strain sensitivity than the same type of sensor that has been reported. When glycerin is filled into the photonic crystal fiber, the strain sensitivity has remained at a high level. The sensitivities significantly increase to 2.98 pm/με and 237.57 pm/°C, respectively. The filling amount can effectively control its sensitivity. Dual-parameter sensitivity matrix is given to prove above conclusion. The proposed sensor has advantages of simple structure, easy to construct and low cost. Furthermore, the sensor can achieve sensitivity requirements by adding different liquids while maintaining polarization.

CRediT authorship contribution statement

Ji Wang: Conceptualization, Validation, Writing - original draft, Writing - review & editing. **Li Pei:** Supervision. **Jianshuai Wang:** Formal analysis. **Zuliang Ruan:** Methodology. **Tigang Ning:** Project administration. **Jingjing Zheng:** Data curation. **Jing Li:** Resources.

Declaration of Competing Interest

The authors declare that they have no known competing financial interests or personal relationships that could have appeared to influence the work reported in this paper.

Acknowledgments

This work is supported by the National Key R&D Program of China (2018YFB1801003) and the National Natural Science Foundation of China (61525501, 61827817).

References

[1] S.M.M. Quintero, A.M.B. Braga, H.I. Weber, A.C. Bruno, J.F.D.F. Araújo, A magnetostrictive composite-fiber Bragg Grating sensor, Sensors 10 (2010) 8119–8128.
[2] C. John, N. Masood, C. Kevin, H. George, Magnetic induction-induced resistive heating of optical fibers and gratings, Opt. Lett. 38 (2013) 926–928.
[3] D. Wu, T. Zhu, M. Deng, D.W. Duan, L.L. Shi, J. Yao, Y.J. Rao, Refractive index sensing based on Mach-Zehnder interferometer formed by three cascaded single-mode fiber tapers, International Conference on Optical Fibre Sensors, 2011, p. 1548.
[4] Z. Tian, S.H. Yam, J. Barnes, W. Bock, P. Greig, J.M. Fraser, H.P. Loock, R.D. Oleschuk, Refractive index sensing with Mach-Zehnder interferometer based on concatenating two single-mode fiber tapers, IEEE Photon. Technol. Lett. 20 (2008) 626–628.
[5] J. Yang, L. Jiang, S. Wang, B. Li, M. Wang, H. Xiao, Y. Lu, H. Tsai, High sensitivity of taper-based Mach-Zehnder interferometer embedded in a thinned optical fiber for refractive index sensing, Appl. Opt. 50 (2011) 5503.
[6] Y.P. Wang, L. Xiao, D.N. Wang, W. Jin, Highly sensitive long-period fiber-grating strain sensor with low temperature sensitivity, Opt. Lett. 31 (2006) 3414.
[7] Z. Tong, J. Zhao, X. Yang, Simultaneous measurement of axial strain and temperature using a PM fiber Bragg grating, Microwave Opt. Technol. Lett. 53 (2015) 867–870.
[8] L. Rindorf, O. Bang, Sensitivity of photonic crystal fiber grating sensors: biosensing, refractive index, strain, and temperature sensing, J. Opt. Soc. Am. B 25 (2008) 310–324.
[9] C. Li, T. Ning, C. Zhang, J. Li, C. Zhang, X. Wen, H. Lin, L. Pei, All-fiber multipath Mach-Zehnder interferometer based on a four-core fiber for sensing applications, Sens. Actuators, A 248 (2016) 148–154.
[10] S. Chowdhury, S. Sen, K. Ahmed, S. Asaduzzaman, Design of highly sensible porous shaped photonic crystal fiber with strong confinement field for optical sensing, Optik 142 (2017) 541–549.
[11] K. Ahmed, M.J. Haque, M.A. Jabin, B.K. Paul, I.S. Amiri, P. Yupapin, Tetra-core surface plasmon resonance based biosensor for alcohol sensing, Physica B 570 (2019) 48–52.
[12] S. Sen, S. Chowdhury, K. Ahmed, S. Asaduzzaman, Design of a porous cored hexagonal photonic crystal fiber based optical sensor with high relative sensitivity for lower operating wavelength, Photon. Sens. 7 (2017) 55–65.
[13] C.W. Wei, C.C. Chan, H. Gong, K.C. Leong, Mach-Zehnder photonic crystal interferometer in cavity ring-down loop for curvature measurement, IEEE Photon. Technol. Lett. 23 (2011) 795–797.
[14] W.C. Wong, C.C. Chan, L.H. Chen, Z.Q. Tou, K.C. Leong, Highly sensitive miniature photonic crystal fiber refractive index sensor based on mode field excitation, Opt. Lett. 36 (2011) 1731–1733.
[15] M.S. Jiang, Q.M. Sui, Z.W. Jin, F.Y. Zhang, L. Jia, Temperature-independent optical fiber Fabry-Perot refractive-index sensor based on hollow-core photonic crystal fiber, Optik – Int. J. Light Electron Opt. 125 (2014) 3295–3298.
[16] J. Zheng, P. Yan, Y. Yu, Z. Ou, J. Wang, X. Chen, C. Du, Temperature and index insensitive strain sensor based on a photonic crystal fiber in line Mach-Zehnder interferometer, Opt. Commun. 297 (2013) 7–11.
[17] M. Sanjida Alam, S. Akter, B. Kumar Paul, K. Ahmed, D. Vigneswaran, M. Nargis Aktar, FEM based highly sensitive dual core temperature sensor: design and analysis, OSA Continuum 2 (2019) 2581–2592.
[18] B.A. Yu, T.J. Ahn, W. Shin, Y.C. Noh, Y.L. Lee, Highly sensitive strain and bending sensor based on a fiber Mach-Zehnder interferometer in photonic crystal fiber, Lasers and Electro-Optics (CLEO) and Quantum Electronics and Laser Science Conference (QELS), 2010 Conference on, 2010, pp. 1–2.
[19] Z. He, Y. Zhu, J. Kaňka, H. Du, Numerical analysis and experimental investigation of highly sensitive photonic crystal fiber long-period grating refractive index sensor, Photonic Crystals and Photonic Crystal Fibers for Sensing Applications III, (2007) pp. 67670E-67670E-67678.
[20] S. Zheng, Y. Zhu, S. Krishnaswamy, Fiber humidity sensors with high sensitivity and selectivity based on interior nanofilm-coated photonic crystal fiber long-period gratings, Sens. Actuators, B 176 (2013) 264–274.
[21] S.A. Mitu, D.K. Dey, K. Ahmed, B.K. Paul, Y. Luo, R. Zakaria, V. Dhasarathan, Fe_3O_4 nanofluid injected photonic crystal fiber for magnetic field sensing applications, J. Magn. Magn. Mater. 494 (2020) 165831.
[22] S. He, X. Dong, S. Jin, J. Guo, High-sensitive temperature sensor based on alcohol-filled highly birefringent photonic crystal fiber loop mirror, Proc. SPIE 7753 (2011) 581–584.
[23] Y. Zhang, Y. Zhao, Z. Li, Simultaneous measuring of magnetic field and temperature based on photonic crystal fiber loop filled with magnetic fluid, Microwave Opt. Technol. Lett. 56 (2014) 2548–2552.
[24] B. Dong, D. Zhou, L. Wei, Temperature insensitive all-fiber compact polarization-maintaining photonic crystal fiber based interferometer and its applications in fiber sensors, J. Lightwave Technol. 28 (2010) 1011–1015.
[25] A. Kumar, N.K. Goel, R.K. Varshney, Studies on a few-mode fiber-optic strain sensor based on LP01-LP 02 mode interference, J. Lightwave Technol. 19 (2002) 358–362.
[26] A. Kumar, R. Jindal, R.K. Varshney, S.K. Sharma, A fiber-optic temperature sensor based on LP 01–LP 02 mode interference, Opt. Fiber Technol. 6 (2000) 83–90.
[27] J. Chen, P. Lu, D. Liu, J. Zhang, S. Wang, D. Chen, Optical fiber curvature sensor based on few mode fiber, Optik 125 (2014) 4776–4778.
[28] L. Li, X. Li, Z. Xie, D. Liu, All-fiber Mach-Zehnder interferometers for sensing applications, Opt. Express 20 (2012) 11109.
[29] Y. Zhou, W. Zhou, C.C. Chan, C.W. Wei, L.Y. Shao, J. Cheng, X. Dong, Simultaneous measurement of curvature and temperature based on PCF-based interferometer and fiber Bragg grating, Opt. Commun. 284 (2011) 5669–5672.
[30] X. Dong, H. Du, Z. Luo, J.A. Duan, Highly sensitive strain sensor based on a novel Mach-Zehnder interferometer with TCF-PCF structure, Sensors 18 (2018) 278.
[31] X. Zhao, M. Dong, Y. Zhang, F. Luo, L. Zhu, Simultaneous measurement of strain, temperature and refractive index based on a fiber Bragg grating and an in-line Mach-Zehnder interferometer, Opt. Commun. 435 (2019) 61–67.
[32] X. Gao, T. Ning, C. Zhang, J. Xu, J. Zheng, H. Lin, J. Li, L. Pei, H. You, A dual-parameter fiber sensor based on few-mode fiber and fiber Bragg grating for strain and temperature sensing, Opt. Commun. 454 (2020) 124441.
[33] J. Villatoro, V. Finazzi, V.P. Minkovich, V. Pruneri, G. Badenes, Temperature-insensitive photonic crystal fiber interferometer for absolute strain sensing, Appl. Phys. Lett. 91 (2007) 091109.
[34] X. Dong, H. Du, X. Sun, J.A. Duan, Simultaneous strain and temperature sensor based on a fiber Mach-Zehnder interferometer coated with Pt by iron sputtering technology, Materials 11 (2018) 1535.